Journal of Sensor Science and Technology
Vol. 31, No. 6 (2022) pp. 383-388
http://dx.doi.org/10.46670/JSST.2022.31.6.383
pISSN 1225-5475/eISSN 2093-7563

# All-Inorganic Metal Halide Perovskite ($CsPbX_3$; X = Cl, Br, I) Nanocrystal-Based Photodetectors

**Junhyuk Ahn[1], Junhyeok Park[1], and Soong Ju Oh[1,+]**

## Abstract

Currently, photodetectors are being extensively studied and developed for next-generation applications, such as in autonomous vehicles and image sensors. In this regard, all-inorganic metal halide perovskite ($CsPbX_3$; X = Cl, Br, and I) nanocrystals (NCs) have emerged as promising building blocks for various applications owing to their high absorption coefficients, tunable bandgaps, high defect tolerances, and solution processability. These features, which are typically required for the development of advanced optoelectronics, can be engineered by modifying the chemical compositions and surface chemistry of the NCs. Herein, we briefly review various strategies adopted for the application of $CsPbX_3$ perovskite NCs in photodetectors and for improving device performance. First, modifications of the chemical compositions of $CsPbX_3$ NCs to tune their optical bandgaps and improve the charge-transport mechanism are discussed. Second, the application of surface chemistry to improve oxidation resistance and carrier mobility is described. In the future, perovskite NCs with prospective features, such as non-toxicity and high resistance to external stimuli, are expected to be developed for practical applications.

**Keywords:** All-Inorganic metal halide perovskites, $CsPbX_3$ nanocrystals, Surface chemistry, Perovskite-based photodetectors, Photodetectors

## 1. INTRODUCTION

Image sensors that convert the variable attenuation of light waves into electrical signals to convey information have emerged as indispensable building blocks for next-generation applications, such as smartphones, aviation technologies, and autonomous vehicles [1–3]. For example, light detection and ranging systems, which employ a laser beam to determine the distance to an object, have been installed in planes for safe landing, paving the way for a significant development in the aviation industry. Furthermore, currently, various photoactive sensors are being gradually incorporated into autonomous vehicles to capture reflected light to immediately detect obstacles and prevent accidents [4,5]. Several research groups have been studying and developing light-capturing materials owing to their high application potential in light-sensing technologies [6,7]. Typically, for the application of photodetectors in real-life devices, a high responsivity and detectivity, a high signal-to-noise ratio, a wide linear dynamic range, wavelength selectivity, and a fast response time are required.

Among various potential candidates, all-inorganic metal halide perovskite ($CsPbX_3$; X = Cl, Br, and I) nanocrystals (NCs) have emerged as promising building blocks for next-generation photodetectors owing to their high light absorption coefficients, high carrier mobilities, long carrier diffusion lengths, high defect tolerances, and high quantum yields [8,9]. In particular, the energy levels of $CsPbX_3$ perovskite NCs can be readily engineered using various post-treatment strategies, owing to their high surface-to-volume ratios and high ion migration rates [10]. Notably, tuning the surface chemistry and/or chemical composition of perovskites induces different optical bandgap energies, leading to wavelength selectivity (Fig. 1) [11]. This tunability is advantageous for the absorption or emission of light within a desired range. For example, the transformation of $CsPbBr_3$ to $CsPbCl_3$ perovskite NCs prevents the absorption of green wavelengths (~550 nm) owing to an increase in the optical bandgap energy. Generally, wavelength selectivity plays a role in reducing the signal-to-noise ratio to improve photodetector performance. Furthermore, $CsPbX_3$ NCs can be readily synthesized via wet chemical methods, including ligand-assisted recrystallization and hot-injection

[1]Department of Materials Science and Engineering, Korea University, Seoul 02841, Republic of Korea
[+]Corresponding author: sjoh1982@korea.ac.kr
(Received: Nov. 13, 2022, Revised: Nov. 24, 2022, Accepted: Nov. 29, 2022)

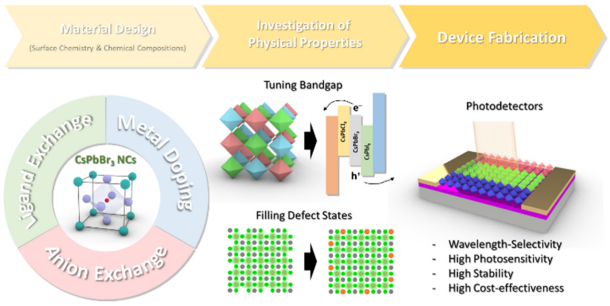


**Fig. 1.** Schematic of the material design and fabrication of $CsPbBr_3$ NC-based photodetectors.

methods [12]. These methods are advantageous for mass production, and the solution processability of NCs leads to cost-effectiveness and allows the fabrication of layer-by-layer structures [13]. Thus, modifying the surface chemistry of $CsPbX_3$ NCs to achieve a high colloidal stability of their inks could facilitate the development of next-generation devices.

## 2. RESULTS AND DISCUSSION

### 2.1 Anion-Exchanged $CsPbX_3$ NC-Based Photodetectors

A conspicuous feature of all-inorganic metal halide perovskite NCs is the tunability of their optical bandgap energy by modifying the chemical compositions. Cation- or anion exchange strategies have been actively applied. Among various methods, the anion exchange method allows for effective composition modifications owing to the fast ion migration rate of halides. Notably, the tunability of the optical bandgap leads to wide-range wavelength detection and light selectivity. In addition, this method allows for the fabrication of cubic $CsPbCl_3$ or $CsPbI_3$ NCs, which cannot be directly synthesized owing to their rapid transformation into orthorhombic or tetragonal phases at room temperature (Fig. 2a). This is because halide ions (Cl, Br, and I) readily diffuse and migrate through the vacancy sites present in perovskite NCs. When bromide ions in $CsPbBr_3$ NCs are exchanged with chloride or iodide, the photoluminescence (PL) peak shifts owing to the change in the optical bandgap energy (Fig. 2b, left). By exploiting these features, several research groups have successfully modulated the properties of perovskite NCs for their applications in photodetectors. For example, Ramasamy et al. added an LiCl or LiI solution to $CsPbBr_3$ NC suspensions to engineer the chemical composition of the NCs [14]. They fabricated visible-range photodetectors using anion-exchanged $CsPbI_3$ NCs and achieved

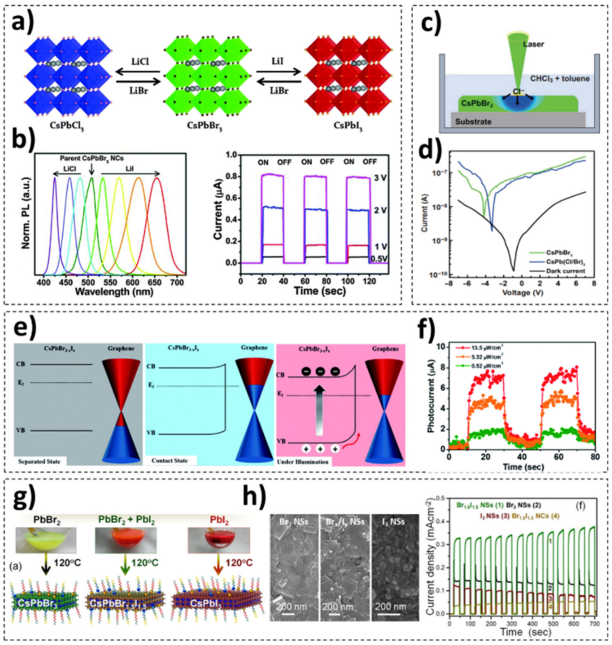


**Fig. 2.** (a) Schematic of the anion-exchange process of $CsPbBr_3$ NCs using LiX in a solution. (b) Normalized PL spectrum of anion-exchanged $CsPbBr_3$ NCs (left), and *I–t* curves (right) of anion-exchanged $CsPbI_3$ NC-based photodetectors (a, b = reprinted with permission from Ref. [14]. Copyright (2016) Royal Society of Chemistry). (c) Schematic of an anion-exchange process with the laser-assisted photolysis of a halocarbon solvent. (d) *I–V* curves of photodetectors based on $CsPbBr_3$ NCs and anion-exchanged $CsPb(Cl/Br)_3$ NCs (c, d = reprinted with permission from Ref. [15]. Copyright (2022) Springer Science + Business Media). (e) Schematic energy diagrams of graphene–$CsPb(Br/I)_3$ NCs in the separated state (left), contact state (middle), and contact under illumination (right). (f) *I–t* curves of graphene–mixed halide perovskite NC-based photodetectors (e, f = reprinted with permission from Ref. [16]. Copyright (2022) Springer Science + Business Media). (g) Photographs and schematic of the as-synthesized (left), mixed halide (middle), and completely anion-exchanged (right) perovskite nanosheets. (h) Scanning electron micrographs (left) and *I–t* curves (right) of $CsPbBr_xI_y$ nanosheet-based photodetectors (g, h = reprinted with permission from Ref. [17]. Copyright (2021) American Chemical Society).

a high on/off ratio (>$10^5$) for the first time (Fig. 2b, right). Xu et al. developed a facile anion-exchange strategy, wherein halide ions were generated via the photolysis of a solvent (Fig. 2c) [15]. By adjusting the laser exposure time of the $CsPbBr_3$ NC films, their compositions were precisely engineered, and the $CsPbBr_3$- and $CsPb(Cl/Br)_3$ NC-based photodetectors exhibited high photoresponsivities at 540 nm and 470 nm, respectively (Fig. 2d).

To further improve the photodetector performance, Kwak et al. incorporated mixed halide perovskite NCs into graphene-based devices (Fig. 2e) [16]. Notably, while pristine graphene-based

devices exhibit p-type doping behavior owing to oxidation, $CsPb(Br/I)_3$ NC-incorporated devices exhibit a negative shift in the Dirac point (Fig. 2f). Because the equilibrium condition at the interfacial layers of the two types of materials provides a better path for charge carriers, the photoresponsivity and response time of the device present improvements. In addition, Mandal et al. reported a method to transform perovskite NCs into nanosheets to improve the photodetector performance (Fig. 2g, h) [17]. The developed two-dimensional photoactive material (nanosheets) exhibited a lower compressive lattice strain and accelerated charge carrier mobility. In addition, by exchanging a small amount of $Br^-$ with $I^-$, the light absorption of the material could be enhanced. Thus, $CsPbBr_{1.5}I_{1.5}$ nanosheet-based photodetectors have achieved better responsivity and detectivity compared to conventional all-inorganic metal halide perovskites.

### 2.2 Metal-Doped $CsPbX_3$ NC-Based Photodetectors

To improve the performance of $CsPbBr_3$ NC-based photodetectors, numerous research groups have engineered the chemical composition of $CsPbBr_3$ NCs by introducing isovalent or heterovalent metal dopants, as depicted in Fig. 3. In this regard, replacing $Pb^{2+}$ in the metal halide perovskites with isovalent dopants, such as $Sn^{2+}$, $Ca^{2+}$, $Sr^{2+}$, $Cd^{2+}$, $Zn^{2+}$, and $Mn^{2+}$, can modify their optical properties or decrease the bandgap [22–24]. Typically, the introduction of trivalent metals, such as $Ce^{3+}$, $Bi^{3+}$, $Sb^{3+}$, $In^{3+}$, $Eu^{3+}$, and $Yb^{3+}$, leads to a longer lifetime and enhanced PL quantum yield owing to the suppression of ionic migration [25]. For example, He et al. synthesized Mn-doped $CsPbBr_3$ NCs by introducing HBr during their synthesis and post-treatment processes to tune the optical bandgap (Fig. 3a) [18]. The addition of HBr did not negatively affect the structural properties of the $CsPbBr_3$ NCs and facilitated the ionization of $MnBr_2$, supplying $Mn^{2+}$ to the NCs. The Mn-doped $CsPbBr_3$ NCs exhibited a longer carrier lifetime, and the Mn-doped $CsPbBr_3$ NC-based photodetectors presented improved photoresponsivity and faster response times than photodetectors based on the as-synthesized $CsPbBr_3$ NCs (Fig. 3b). Wang et al. reported that $Zn^{2+}$ doping played a role in decreasing the number of defects in $CsPbBr_3$ NCs (Fig. 3c, d) [19]. The dopant optimized the carrier-trapping process and weakened the "overshoot" phenomenon, that is, the appearance of sharp transient peaks in the photocurrent curves owing to rapid changes in the incident light signal.

Furthermore, the effects of trivalent dopants on the properties of the $CsPbBr_3$ NCs have been investigated. Subramaniam et al. reported a strategy to introduce $Sb^{3+}$ into $CsPbBr_3$ NCs to fill halide

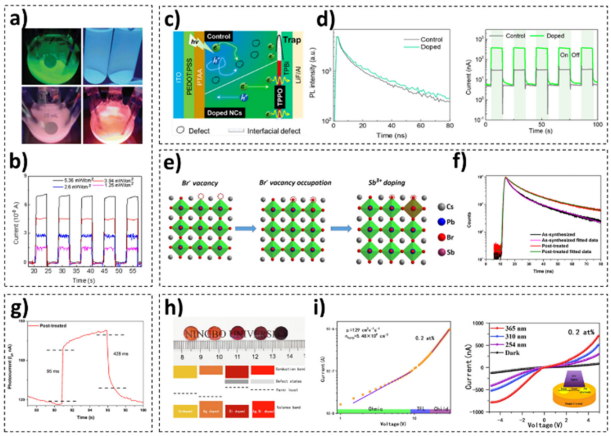


**Fig. 3.** (a) Images of the as-synthesized (green), HBr-added (blue), Mn-doped (with HBr) (pink), and Mn-doped (with a larger amount of HBr) colloidal $CsPbBr_3$ NCs. (b) Performance of photodetectors based on Mn-doped $CsPbBr_3$ NCs (a, b = reprinted with permission from Ref. [18]. Copyright (2021) Springer Science + Business Media). (c) Schematic of the reduced "overshoot" phenomenon. (d) Time-resolved PL curves (left) and *I–t* curves (right) of the as-synthesized and Zn-doped $CsPbBr_3$ NCs (c, d = reprinted with permission from Ref. [19]. Copyright (2021) American Chemical Society). (e) Schematic of defect passivation and the $Sb^{3+}$-doping mechanism. (f) Time-resolved PL curves of the as-synthesized and Mn-doped $CsPbBr_3$ NCs, and (g) photodetector response of the Mn-doped $CsPbBr_3$ NCs (e-g = reprinted with permission from Ref. [20]. Copyright (2022) American Chemical Society). (h) Photographs of polished 0, 0.2, 0.25, 0.4, and 1.0 at% $Ag^+/Bi^{3+}$ co-doped $CsPbBr_3$ NCs on wafers (upper), and schematic of the Fermi level, defect state density, valence, and conduction band edge position (lower). (i) log*I*–log*V* curves (left) and *I–V* curves (right) of 0.2 at% $Ag^+/Bi^{3+}$ co-doped $CsPbBr_3$ NCs (h, i = reprinted with permission from Ref. [21]. Copyright (2022) Elsevier).

vacancies (Fig. 3e) [20]. Because the $Sb^{3+}$ species occupied the defect sites of the $Br^-$ vacancies on the $CsPbBr_3$ NC surface, the carrier lifetime and PL quantum yield increased (Fig. 3f). Owing to the reduced number of defective surface sites, the response times of the Sb-doped $CsPbBr_3$ NC-based photodetectors were significantly enhanced (Fig. 3g). Gong et al. proposed an $Ag^+/Bi^{3+}$ co-doping strategy to prevent a decrease in the concentration of defect states and changes in the Fermi level, which were caused by the introduction of $Bi^{3+}$ as a single dopant (Fig. 3h) [21]. Although metal dopants play a role in decreasing the number of defect sites, the optical bandgap energy can also change owing to changes in the chemical composition or structural distortions. To resolve these issues, Gong et al. introduced another metal dopant, $Ag^+$, into $CsPbBr_3$ crystals using the vertical Bridgman technique, thereby successfully controlling the bandgap energy and improving the performance of $CsPbBr_3$ NC-based photodetectors (Fig. 3i).

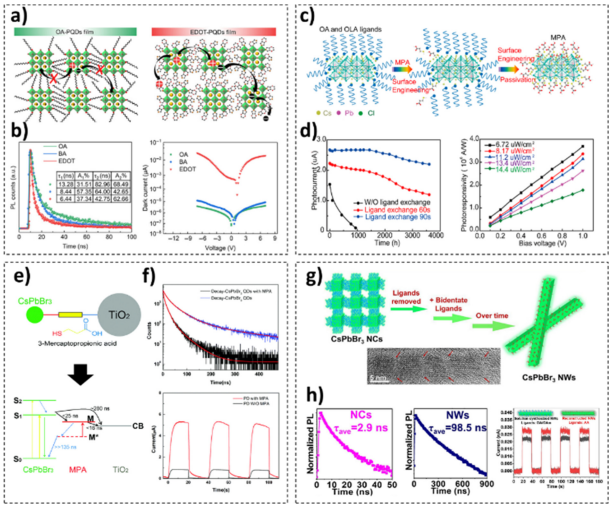

**Fig. 4.** (a) Schematic of the carrier transport in solid films of (left) oleic acid-passivated and (right) EDOT-passivated $CsPbBr_3$ NCs. (b) Time-resolved PL curves (left) and *I–V* curves (right) (a, b = reprinted with permission from Ref. [26]. Copyright (2021). Springer Science + Business Media). (c) Schematic of the surface passivation process, wherein the oleate ligands are replaced with MPA ligands. (d) Photocurrent measured using $CsPbCl_3$ NC-based photodetectors without and with passivation under ambient conditions (left), and photoresponsivity as a function of the bias voltage at different intensities of 400 nm light (right) (c, d = reprinted with permission from Ref. [27]. Copyright (2019) American Chemical Society). (e) Schematic illustrating the excitation process in a $CsPbBr_3$ NC-MPA-$TiO_2$ system following light irradiation. (f) Time-resolved PL spectra (upper) and *I–t* curves (lower) of $CsPbBr_3$ quantum dot films without and with MPA treatment (e, f = reprinted with permission from Ref. [28]. Copyright (2017) Royal Society of Chemistry). (g) Schematic of the transformation of $CsPbBr_3$ NCs to nanowires through a ligand-exchange strategy. (h) Time-resolved PL spectra of $CsPbBr_3$ (left) NCs and nanowires (middle), and *I–t* curves of the $CsPbBr_3$ NCs and NWs (g, h = reprinted with permission from Ref. [29]. Copyright (2022) American Chemical Society).

### 2.3 Surface-Modified $CsPbX_3$ NC-Based Photodetectors

Typically, zero-dimensional nanomaterials, such as NCs and quantum dots, require surface modification strategies, such as ligand exchanges, to improve their oxidation stability and physical properties [30]. The stability and physical properties of NCs can be determined based on their lengths and the functional (terminal) groups of their surface ligands [31]. Yan et al. reported that a conductive polymer ligand, 3,4-ethylenedioxythiophene (EDOT), improved the photocurrent response of $CsPbBr_3$ NC-based photodetectors by enhancing carrier transport (Fig. 4a) [26]. This was because the lone pair electrons on the S atoms of EDOT passivated the defects on the surface of the $CsPbBr_3$ NCs (Fig. 4b). In addition, the conjugated structure of the benzene ring of EDOT improved the stability of NCs. Gong et al. exploited 3-mercaptopropionic acid (MPA) as a ligand to improve the air stability (oxidation resistance) of $CsPbX_3$ NCs (Fig. 4c) [27]. They observed that the MPA ligand-passivated $CsPbCl_3$ NCs exhibited higher sustainability under ambient conditions, despite the lower steric hindrance of MPA compared to that of the oleate ligand (Fig. 4d). This is because the –SH groups are coupled electronically with the $CsPbCl_3$ NCs, preventing the degradation in charge transfer.

Several research groups have reported that the ligand exchange of $CsPbBr_3$ NCs is beneficial for the implementation of other surface modification strategies. Zhou et al. employed MPA ligands as bifunctional linkers to capture $TiO_2$ nanoparticles on a $CsPbBr_3$ NC surface (Fig. 4e) [28]. The thiol (–SH) and carboxylate (–COOH) groups of MPA interacted with the $CsPbBr_3$ NC and $TiO_2$ nanoparticles, respectively; therefore, the $TiO_2$ nanoparticles tethered to the NC surface. Because the excited electrons were transferred from the $CsPbBr_3$ NCs to the MPA ligand and then to the $TiO_2$ nanoparticles, the decay time of the carriers decreased (Fig. 4f). Zhao et al. reported that treatment with aminocaproic acid ligands allowed the transformation of $CsPbBr_3$ NCs into $CsPbBr_3$ nanowires (Fig. 4g) [29]. The change in the dimensions of the material from zero to one via anisotropic growth contributed to a decrease in the number of defect sites, leading to an improved on/off ratio of the photodetector (Fig. 4h).

## 3. CONCLUSIONS

Herein, we reviewed various strategies adopted for realizing all-inorganic metal halide perovskite ($CsPbX_3$; X = Cl, Br, and I) NC-based photodetectors with improved performance. Notably, the outstanding features of $CsPbX_3$, including its high absorption coefficient, tunable optical bandgap energy, improved stability, and solution processability, have facilitated the development of state-of-the-art photodetectors. To exploit these versatile features, several research groups have modified the surface chemistries and engineered the stoichiometry of $CsPbBr_3$ NCs. The various strategies employed have not only aided the development of solution-processed photodetectors with wavelength selectivity, high sensitivity, and high oxidative resistance but also provided fundamental insights into perovskite NCs. However, although the performance of the photodetectors could be significantly

improved using various strategies, further requirements, particularly the NC stability, should be considered for the real-life application of $CsPbX_3$ NCs. If stability studies are carefully conducted in parallel with property engineering, all-inorganic metal halide perovskite NCs could be commercialized and utilized in real-life applications, such as smartphones and autonomous vehicles, in the future.

## ACKNOWLEDGEMENTS

This study was financially supported by the Creative Materials Discovery Program through the National Research Foundation (NRF) of Korea funded by the Ministry of Science and ICT (NRF-2018M3D1A1059001), the Materials Innovation Project (NRF-2021M3H4A3026733), the Ministry of Science, ICT, and Future Planning (2022R1A2C4001517), and the BK21 FOUR Program through the NRF funded by the Ministry of Education (4199990514635).

## REFERENCES

[1] S. Biswas, Y. Lee, and H. Kim, "Micropower energy harvesting using high-efficiency indoor organic photovoltaics for self-powered sensor systems", *J. Sens. Sci. Technol.*, Vol. 30, No. 6, pp. 364-368, 2021.

[2] X. Meng, J. Yang, C. Zhang, Y. Fu, K. Li, M. Sun, X. Wang, C. Dong, B. Ma, and Y. Ding, "Light-Driven $CO_2$ Reduction over Prussian Blue Analogues as Heterogeneous Catalysts", *ACS Catal.*, Vol. 12, No. 1, pp. 89-100, 2022.

[3] C. Debeunne and D. Vivet, "A Review of Visual-LiDAR Fusion based Simultaneous Localization and Mapping", *Sens.*, Vol. 20, No. 7, pp. 2068(1)-2068(20), 2020.

[4] D. Jayachandran, A. Oberoi, A. Sebastian, T. H. Choudhury, B. Shankar, J. M. Redwig, and S. Das, "A low-power biomimetic collision detector based on an in-memory molybdenum disulfide photodetector", *Nat. Electron*, Vol. 3, No. 10, pp. 645-655, 2020.

[5] N. Lee, S. Kwon, and H. Ryu, "Adaptive Obstacle Avoidance Algorithm using Classification of 2D LiDAR Data", *J. Sens. Sci. Technol.*, Vol. 29, No. 5, pp. 348-353, 2020.

[6] H. Kwen, S. Kim, J. Lee, P. Choi, and J. Shin, "Simulation of High-Speed and Low-Power CMOS Binary Image Sensor Based on Gate/Body-Tied PMOSFET-Type Photodetector Using Double-Tail Comparator", *J. Sens. Sci. Technol.*, Vol. 29, No. 2, pp. 82-88, 2020.

[7] J. Lee, B. Choi, D. Seong, J. Lee, S. Kim, J. Lee, J. Shin, and P. Choi, "CMOS Binary Image Sensor with Gate/Body-Tied PMOSFET-Type Photodetector for Low-Power and Low-Noise Operation", *J. Sens. Sci. Technol.*, Vol. 27, No. 6, pp. 362-367, 2018.

[8] S. Ullah, J. Wang, P, Yang, L. Liu, S. Yang, T. Xia, H. Guo, and Y. Chen, "All-inorganic $CsPbBr_3$ perovskite: a promising choice for photovoltaics", *Mater. Adv.*, Vol. 2, No. 2, pp. 646-683, 2021.

[9] X. Du, G. Wu, J. Cheng, H. Dang, K. Ma, Y. Zhang, P. Tan, and S. Chen, "High-quality $CsPbBr_3$ perovskite nanocrystals for quantum dot light-emitting diodes", *RSC Adv.*, Vol. 7, No. 17, pp. 10391-10396, 2017.

[10] L. Protesescu, S. Yakunin, M. I. Bodnarchuk, F. Krieg, R. Caputo, C. H. Hendon, R. X. Yang, A. Walsh, and M. V. Kovalenko, "Nanocrystals of Cesium Lead Halide Perovskites ($CsPbX_3$, X = Cl, Br, and I): Novel Optoelectronic Materials Showing Bright Emission with Wide Color Gamut", *Nano Lett.*, Vol. 15, No. 6, pp. 3692-3696, 2015.

[11] J. Ahn, Y. M. Lee, W. Kim, S. Y. Lee, J. H. Bae, J. Bang, and S. J. Oh, "Investigation of the Role of Cations during Anion Exchange in All-Inorganic Halide Perovskite Nanocrystals", *ESC J. Solid State Sci. Technol.*, Vol. 10, No. 10, p. 106003, 2021.

[12] W. Kim, S. Jeon, and S. J. Oh, "Wearable sensors based on colloidal nanocrystals", *Nano Convergence*, Vol. 6, No. 10, pp. 1-13, 2019.

[13] J. Bang, J. Ahn, and S. J. Oh, "Designing a nanocrystal-based temperature and strain multi-sensor with one-step inkjet printing", *J. Sens. Sci. Technol.*, Vol. 30, No. 4, pp. 218-222, 2021.

[14] P. Ramasamy, D. Lim, B. Kim, S. Lee, M. Lee, and J. Lee, "All-inorganic cesium lead halide perovskite nanocrystals for photodetector applications", *Chem. Commun.*, Vol. 52, No. 10, pp. 2067-2070, 2016.

[15] X. Xu, Y. Dong, Y. Zhang, Z. Han, J. Liu, D. Yu, Y. Wei, Y. Zou, B. Huang, J. Chen, and H. Zeng, "High-definition colorful perovskite narrowband photodetector array enabled by laser-direct-writing", *Nano Research*, Vol. 15, No. 6, pp. 5476-5482, 2022.

[16] D. Kwak, D. Lim, H. Ra, P. Ramasamy, and J. Lee, "High performance hybrid graphene-$CsPbBr_{3-x}I_x$ perovskite nanocrystal photodetector", *RSC Adv.*, Vol. 6, No. 69, pp. 65252-65256, 2016.

[17] A. Mandal, A. Ghosh, D. Ghosh, and S. Bhattacharyya, "Photodetector with High Responsivity by Thickness Tunable Mixed Halide Perovskite Nanosheets", *ACS Appl. Mater. Interfaces*, Vol. 13, No. 36, pp. 43104-43114, 2021.

[18] W. He, Q. Zhang, Y. Qi, J. Xiong, P. Ray, N. R. Pradhan, T. V. Shahbazyan, F. Han, and Q. Dai, "Luminescence properties of $CsPbBr_3$:Mn nanocrystals", *J. Nanopart. Res.*, Vol. 23, No. 80, pp. 1-9, 2021.

[19] T. Wang, T. Fang, X. Li, L. Xu, and J. Song, "Controllable Transient Photocurrent in Photodetectors Based on Perovskite Nanocrystals via Doping and Interfacial Engineering", *J. Phys. Chem. C*, Vol. 125, No. 10, pp. 5475-5484, 2021.

[20] M. R. Subramaniam, A. K. Pramod, S. A. Hevia, and S. K. Batabyal, "Enhanced Photoluminescence Quantum Yield, Lifetime, and Photodetector Responsivity of $CsPbBr_3$ Quantum Dots via Antimony Tribromide Post-Treatment", *J. Phys. Chem. C*, Vol. 126, No. 3, pp. 1462-1470, 2022.

[21] Z. Gong, W. Zhang, S. Pan, and J. Pan, "$Ag^+/Bi^{3+}$ doping

induced band structure and optoelectronic properties changes in $CsPbBr_3$ crystals", *J. Crystal Growth*, Vol. 586, pp. 126604(1)-126604(8), 2022.

[22] D. Parobek, Y. Dong, T. Qiao, and D. H. Son, "Direct Hot-Injection Synthesis of Mn-Doped $CsPbBr_3$ Nanocrystals", *Chem. Mater.*, Vol. 30, No. 9, pp. 2939-2944, 2018.

[23] J. Navas, A. S. Coronilla, J. J. Gallardo, N. C. Hernandez, J. C. Pinero, R. Alcantara, C. F. Lorenzo, D. M. Santos, T. Aguilar, and J. M. Calleja, "New insights into organic-inorganic hybrid perovskite $CH_3NH_3PbI_3$ nanoparticles. An experimental and theoretical study of doping in $Pb^{2+}$ sites with $Sn^{2+}$, $Sr^{2+}$, $Cd^{2+}$ and $Ca^{2+}$", *Nanoscale*, Vol. 7, No. 14, pp. 6216-6229, 2015.

[24] W. Stam, J. J. Geuchies, T. Altantzis, K. H. Bos, J. D. Meeldijk, S. V. Aert, S. Bals, D. Vanmaekelbergh, and C. D. Donega, "Highly Emissive Divalent-Ion-Doped Colloidal CsPb1-xMxBr3 Perovskite Nanocrystals through Cation Exchange", *J. Am. Chem. Soc.*, Vol. 139, No. 11, pp. 4087-4097, 2017.

[25] S. Jung, J. H. Kim, J. W. Choi, J. Kang, S. Jin, Y. Kang, and M. Song, "Enhancement of Photoluminescence Quantum Yield and Stability in $CsPbBr_3$ Perovskite Quantum Dots by Trivalent Doping", *Nanomater.*, Vol. 10, No. 4, , pp. 710(1)-710(10), 2020.

[26] W. Yan, J. Shen, Y. Zhu, Y. Gong, J. Zhu, Z. When, and C. Li, "$CsPbBr_3$ quantum dots photodetectors boosting carrier transport via molecular engineering strategy", *Nano Research*, Vol. 14, No. 11, pp. 4038-4045, 2021.

[27] M. Gong, R. Sakidja, R. Goul, D. Ewing, M. Casper, A. Stramel, A. Elliot, and J. Z. Wu, "High-Performance All-Inorganic $CsPbBr_3$ Perovskite Nanocrystal Photodetectors with Superior Stability", *ACS Nano*, Vol. 13, No. 2, pp. 1772-1783, 2019.

[28] L. Zhou, K. Yu, F. Yang, H. Cong, N. Wang, J. Zheng, Y. Zuo, C. Li, B. Cheng, and Q. Wang, "Insight into the effect of ligand-exchange on colloidal $CsPbBr_3$ perovskite quantum dot/mesoporous-$TiO_2$ composite-based photodetectors: much faster electron injection", *J. Mater. Chem. C*, Vol. 5, No. 25, pp. 6224-6233, 2017.

[29] C. Zhao, Z. He, P. Wangyang, J. Tan, C. Shi, A. Pan, L. He, and Y. Liu, "Bidentate Ligand-Induced Oriented Transformation of $CsPbBr_3$ Perovskite Nanocrystals into Nanowires for X-ray Photodetectors", *ACS Appl. Nano Mater.*, Vol. 5, No. 10, pp. 13737-13744, 2022.

[30] M. A. Boles, D. Ling, T. Hyeon, and D. V. Talapin, "The surface science of nanocrystals", *Nat. Mater.*, Vol. 15, No. 2, pp. 141-153, 2016.

[31] Z. Pang, J. Zhang, W. Cao, X. Kong, and X. Peng, "Partitioning surface ligands on nanocrystals for maximal solubility", *Nat. Commun.*, Vol. 10, No. 1, pp. 1-8, 2019.